論文 / 著書情報
Article / Book Information

Title	An Innovative Fuel Design for HTGRs: Evaluating a 10-Hour High-Temperature Oxidation of the SiC Fuel Matrix During Air Ingress Accident Conditions
Authors	Yosuke Nishimura, Anna Gubarevich, Katsumi Yoshida, Koji Okamoto
Citation	Energies, Vol. 17, Issue 21,
Pub. date	2024, 10
Creative Commons	The information is in the article.

energies

MDPI

Article

An Innovative Fuel Design for HTGRs: Evaluating a 10-Hour High-Temperature Oxidation of the SiC Fuel Matrix During Air Ingress Accident Conditions

Yosuke Nishimura [1,*], Anna Gubarevich [2], Katsumi Yoshida [2,*] and Koji Okamoto [1]

[1] The Department of Nuclear Engineering and Management, Graduate School of Engineering, The University of Tokyo, 7-3-1, Hongo, Bunkyo-Ku, Tokyo 113-8654, Japan; okamoto@n.t.u-tokyo.ac.jp
[2] Laboratory for Zero-Carbon Energy, Institute of Innovative Research, Tokyo Institute of Technology, 2-12-1, Ookayama, Meguro-Ku, Tokyo 152-8550, Japan; hubarevich.h.aa@m.titech.ac.jp
* Correspondence: nishimura-y@g.ecc.u-tokyo.ac.jp (Y.N.); k-yoshida@zc.iir.titech.ac.jp (K.Y.); Tel.: +81-80-6890-4535 (Y.N.)

Abstract: Preventing severe corrosion incidents caused by air ingress accidents in high-temperature gas-cooled reactors (HTGRs) while improving heat removal efficiency from the core is of paramount importance. To enhance both safety and efficiency, a sleeveless silicon carbide (SiC)-matrix fuel compact has been proposed. This study evaluates the 10-hour oxidation of reaction-sintered SiC (RS-SiC)-matrix fuel compact under the conditions of an air ingress accident within the temperature range of 1000 to 1400 °C. The oxidation tests were conducted in a stagnant air environment without flow. As a result, it is demonstrated that RS-SiC exhibits exceptional resistance to air oxidation up to 1400 °C, as shown by the thermogravimetric analysis (TGA), with minimal mass loss due to the oxidation of free carbon. Scanning electron microscopy with energy-dispersive X-Ray spectroscopy (SEM–EDX) analysis reveals that the morphology and thickness of the SiO_2 layer formed on the RS-SiC surface vary with temperature. At 1400 °C, uniform oxide layer thickness ranging from 1.59 to 4.10 μm and localized nodule-like oxide formations of approximately 10 μm are observed. In contrast, at 1000–1200 °C, thinner oxide layers are identified, indicating that oxide growth accelerates at higher temperatures. The oxidation rates measured provide insights into the mechanisms of oxide growth.

Keywords: silicon carbide; reaction sintering; oxidation; corrosion resistance; high-temperature gas-cooled reactor (HTGR)

Citation: Nishimura, Y.; Gubarevich, A.; Yoshida, K.; Okamoto, K. An Innovative Fuel Design for HTGRs: Evaluating a 10-Hour High-Temperature Oxidation of the SiC Fuel Matrix During Air Ingress Accident Conditions. *Energies* **2024**, *17*, 5366. https://doi.org/10.3390/en17215366

Academic Editor: Guglielmo Lomonaco

Received: 4 September 2024
Revised: 22 October 2024
Accepted: 25 October 2024
Published: 28 October 2024

1. Introduction

It has become increasingly evident that nuclear energy holds immense potential as a sustainable and clean source of power worldwide, capable of meeting the ever-growing global energy demands [1]. The high-temperature gas-cooled reactor (HTGR) stands out among nuclear technologies due to its inherent safety features that reduce the risk of core melting, its potential to generate hydrogen for industrial use, and its ability to safely and efficiently consume plutonium from Light Water Reactor spent fuel, offering a solution for nuclear waste management. Studies also show that Pu-burner HTGRs achieve better burnup than uranium fuel-loaded reactors [2,3]. These positive characteristics have captured global attention, positioning HTGRs as promising candidates for the next generation of reactors worldwide.

To facilitate commercial application, it is essential to enhance the core power density during normal operation and ensure safety during abnormal events [4,5]. The fundamental reactor core design of pin-in-block type HTGRs has remained unchanged for the past 30 years [6]. In the current design, a graphite sleeve is employed as a chemical barrier against corrosion of a graphite-matrix fuel; meanwhile, this sleeve limits the allowable thermal power output from the core due to the thermal resistance of a gap between the

sleeve and the fuel matrix, preventing the maximum fuel temperature from exceeding its acceptable design limit [7].

To address these challenges and improve the overall efficiency, a new fuel design has been proposed using silicon carbide (SiC) ceramics as a replacement for the fuel matrix, thereby eliminating the need for the sleeve [8–12]. Removing the sleeve would decrease thermal resistance and allow the fuel compact to be in direct contact with the helium coolant. Figure 1 illustrates the concept of the proposed sleeveless design and its supporting method, which involves the use of spacers [9]. In addition, assume a case where the flow distribution ratio between the inner and outer channels of the fuel compact can be adjusted by modifying the shape of the spacers. In the newly proposed design, the fuel compact can be cooled down both from the central and outer sides (between the fuel compact and the graphite core block) under normal power operation. The coolant pass region is widespread. This makes it possible to improve the heat removal efficiency; thus, a higher power density operation will be achievable.

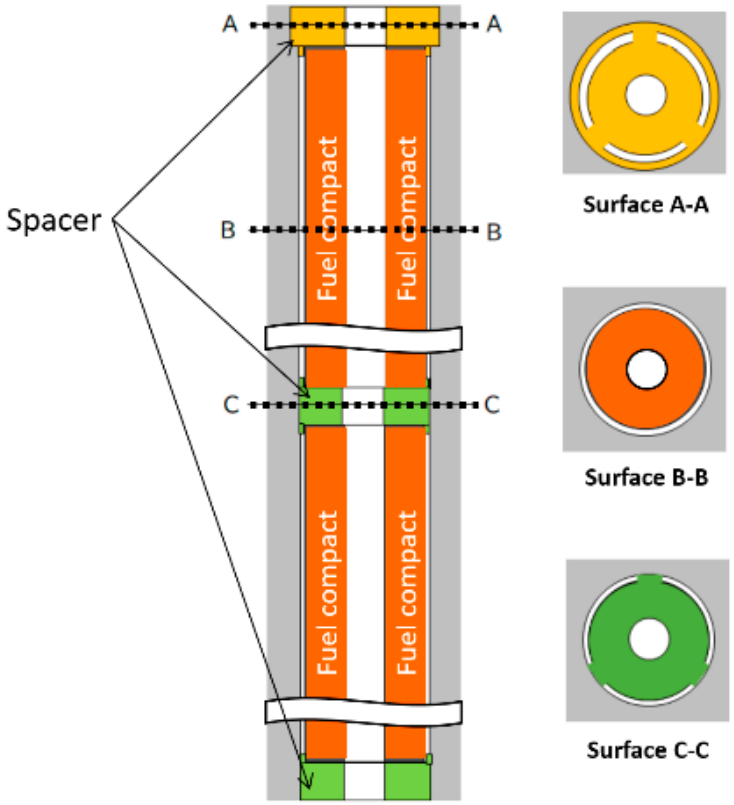

Figure 1. Schematic view of sleeveless fuel compacts supported by some spacers.

In the previous fuel design, the graphite sleeve was intended to serve as a chemical buffer against oxidation; however, in the sleeveless fuel design, the fuel matrix is naked and exposed to gases. This implies that the use of graphite as a fuel matrix is not viable due to its susceptibility to oxidation, which could result in the deterioration of the fuel integrity. Therefore, an alternative material is required instead of graphite. In this context, SiC has garnered interest in extreme environments, including nuclear reactors, due to its high mechanical strength, thermal conductivity, and chemical stability [13]. With the proposed sleeveless fuel compacts design (Figure 2), the fuel matrix needs great anticorrosion properties to protect the TRISO fuel particles embedded in the fuel matrix, particularly in the event of an air ingress accident arising from a guillotine-type break of the main coolant pipe [14–17] that leads to severe mechanical and material degradation of the core structures and fuel compacts due to high temperature oxidation [18–21].

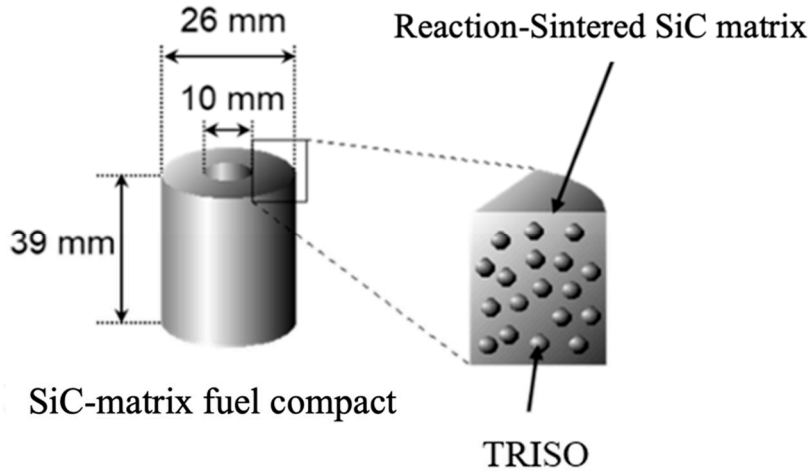

Figure 2. Conceptual illustration of the size and internal view of the SiC-matrix fuel compact.

In the design of an accident-tolerant fuel (ATF), fully ceramic microencapsulated (FCM) fuel [22–28] utilizes SiC ceramics for their excellent ability to protect the fuel matrix during LWR accident conditions. Recently, the design has been employed commercially in the Micro Modular Reactor (MMR) of Ultra Safe Nuclear Corporation. As for the fuel waste management, although direct disposal seems to be the most reasonable option for TRISO spent fuel, conducting studies on reprocessing is also important, given the economic and environmental determinants of the future and the circular economy requiring the recovery of nuclear resources and reducing the amount of disposed waste. The management of spent sleeveless fuel is expected to reduce graphite waste production. The detached compacts or TRISO particles can be directed to storage or reprocessed for U and Pu recovery [29]. Guittonneau et al. proposed a method [30] that allows the total degradation of graphite blocks and the separation of TRISO particles while maintaining their cohesion. The method was based on the intercalation of sulfuric acid into graphite layers to separate the grains. It was found that a good partition of the TRISO grains from the graphite-matrix of compacts occurs through acid treatment. Similar to this method, it must be noted that the treatment allows for preventing damage to the spent TRISO fuel particles during the process of removing TRISO particles from the SiC-matrix in the proposed design.

SiC not only resists steam oxidation but also maintains a stable "passive mode" during dry oxidation at high temperatures [31].

$$\mathrm{SiC} + \frac{3}{2}\mathrm{O_2} \rightarrow \mathrm{SiO_2\ (s)} + \mathrm{CO\ (g)} \quad (1)$$

During an air ingress event, the passive behavior of SiC significantly contributes to protecting the fuel matrix by forming an oxide layer that prevents corrosion. From the perspective of fuel safety, SiC oxidation in passive mode plays a key role in preventing the radioactive release from the fuel matrix to the environment in the case of accidents; thus, the SiC fuel matrix greatly helps the safety of HTGRs. The oxidation characteristics of SiC largely depend on its crystal structure and fabrication process [32]. The previous investigation addresses the oxidation behaviors that have been widely discussed but lack consensus due to the different types of SiC and experimental variables. In our proposed design, we have chosen the reaction sintering process for fuel fabrication. This is because various conventional methods [33–36], such as pressure-less sintering, hot pressing, hot isostatic pressing, chemical vapor deposition, spark plasma sintering, and nano-infiltration transient eutectic-phase (NITE) formation process [37], are unsuitable for the SiC fuel matrix in HTGRs. The high mechanical pressure and temperature conditions involved in these processes pose a risk of severe damage to the TRISO-coated fuel particles embedded in the matrix. It is crucial to investigate the oxidation kinetics of reaction-sintered SiC

(RS-SiC) to assess fuel safety in the event of accidents. However, there is currently a lack of comprehensive understanding of the fundamental kinetics of the RS-SiC oxidation.

In our previous study, thermogravimetric tests demonstrated that graphite experiences severe weight loss at elevated temperatures, while SiC follows a passive oxidation mode with a slight weight gain up to 1400 °C. The Deal–Grove model was observed in the SiC's oxidation kinetics, with an activation energy of 323 kJ/mol, indicating SiC's superior oxidation resistance compared to graphite [8]. The next research validated the oxidation behavior of real-scale SiC fuel compacts under HTGR air ingress conditions using integrated experiments and CFD simulations. SiC exhibited passive oxidation at both 900 °C and 1100 °C, with slightly reduced weight gain at higher temperatures, indicating potential damage to the SiO_2 layer. The experiments confirmed the absence of active oxidation mode at oxygen concentrations above 10 ppm and temperature values below 1100 °C, ensuring the safe use of SiC fuel compacts within these parameters [11]. The last study focused on the passive/active oxidation transition of RS-SiC at high temperatures. We identified the passive-to-active transition under specific conditions, particularly at 1400 °C and low oxygen concentrations. The proposed kinetic model described the SiO_2/SiC interface reaction, crucial for preventing active oxidation, which could lead to severe material degradation [12].

This study will focus on the mechanism of oxide growth on RS-SiC, as estimating the oxide thickness is important for safety evaluation. The main objectives are to investigate the oxide structure of the SiC fuel matrix and to elucidate the oxidation kinetics during the postulated accidents to support the development of the innovative fuel design with enhanced thermal efficiency and safety for future HTGR applications.

2. Experimental Details

Aiming to evaluate the oxidation behavior of SiC fuel matrix, commercially available reaction-sintered SiC matrices (RS-SiC) (Sato Tekko Co., Ltd., Chiba, Japan) were used as test samples. X-Ray diffraction (XRD) study detected less free crystalline Si phase in this sample [8]. The samples were cut from SiC balls to form cylinders (average D = 3.01 mm, H = 2.65 mm, and W = 56.72 mg). The samples were cleaned before testing in acetone under ultrasonic treatment and then dried in air.

The oxidation tests of the samples were conducted using Thermogravimetry Differential Thermal Analysis (TG-DTA, Bruker, MA, USA, model TG-DTA2020SA). The temperature was elevated from room temperature (27 °C) to the targeted temperatures at a constant rate of 20 °C/min under atmospheric pressure. The air oxidation process was observed for 10 h at a constant temperature within the range of 1000~1400 °C for replicating accidental conditions [15]. In an accident, the fuel temperature rises due to the loss of helium coolant. After the scram, decay heat from the core would be the primary reason for the temperature rise, and reaction heat from fuel oxidation also accelerates the heating. The oxidation tests were conducted in stagnant environment without flow. Even though the flow conditions are different from the actual accident, we believe that the flow effect is negligible. In fact, we have previously demonstrated that there is not a large difference in oxidation rates between stagnant air and air flow [8,12]. In this experiment, temperature has a huge impact on SiC oxidation behaviors as a main parameter, not flow rate. Moreover, the air ingress accident progresses very slowly via molecular diffusion [38], which means that the air comes through the reactor core in almost stagnant environment after Loss-Of-Coolant Accident (LOCA) and depressurization caused by guillotine-type break of the primary coolant pipes. Therefore, we believe that the experimental conditions can be representative of the accidental environment. The mass changes were measured at real-time monitoring with 1.0 sec sampling time for 10 h. The accuracy of the mass change measurement was 0.1 μg.

Crystalline phases were determined using XRD method (XRD, Aeris, Malvern Panalytical, Eindhoven, The Netherlands). For the microstructure observation, field emission scanning electron microscope (FE-SEM; S-4800, Hitachi High-Tech Corporation, Tokyo,

Japan) equipped with energy dispersive X-Ray spectroscopy (EDX) detector (EDAX, active area 300 mm^2) was used. The accelerating voltage was 5.0 kV. The samples after oxidation tests were mounted in epoxy resin, then cut or ground to expose the SiC–SiO_2 interface and coated with a thin layer of platinum to prevent electron charging.

3. Results and Discussion

Figure 3 shows the XRD pattern of the RS-SiC sample after oxidation at 1400 °C. Before the oxidation, the sample consisted of α and β SiC mixture [8]; after oxidation, SiO_2 in cristobalite form was formed on the surface as indicated. The microstructure of the oxidized samples was investigated through FE-SEM observation. For specifying the chemical compounds of the product, SEM–EDX mapping data highlight the existence of SiO_2, reflecting the Si, O composition profile as presented. In Figures 4–6, cross-sectional images of microstructures are provided, focusing on the resin/SiC interface for characterizing the oxide structure. Small and large particle structures can be recognized that are typical polycrystalline structures for reaction-sintered SiC consisting of α-β mixed matrix with a large crack running through the surface. Crack formation was probably due to compressive stress caused by thermal shock applied to the oxide/SiC interface. In the sample case at 1400 °C, a uniform oxide layer was detected on the SiC surface with a thickness of approximately 1.59–4.10 μm (Figure 4a,b). A nodule-like oxide product was also found on the SiC surface (Figure 4c). From the cross-sectional view, the thickness and width of the nodule-like product were measured to be approximately 10 and 80 μm, respectively. Due to its polycrystalline structure and rough surface, RS-SiC showed nonhomogeneous oxide growth, leading to the local formation of thick nodule-like oxide and a thin uniform oxide layer in different areas. At 1200 °C (Figure 5a,b), thin oxide layers (2.7 μm in average) were identified with relatively large pores in the matrix. In general, SiC contains pores, which make it easier for oxygen to diffuse through open pores. At 1000 °C (Figure 6a,b), thinner oxide layers were detected with less than 1.3 μm thickness. From Figures 4–6, it was confirmed that oxide growth is accelerated under elevated temperatures up to 1400 °C for 10 h duration. During the oxidation, no corrosion was identified due to protective passive oxidation with the formation of dense oxide layers, which contributes to the nuclear fuel safety during accidents.

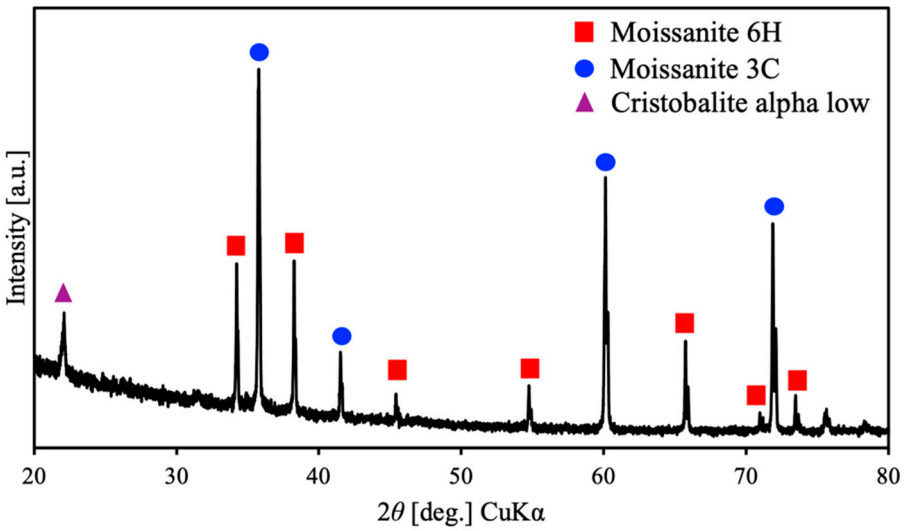

Figure 3. XRD pattern of the RS-SiC sample after oxidation test in air at 1400 °C.

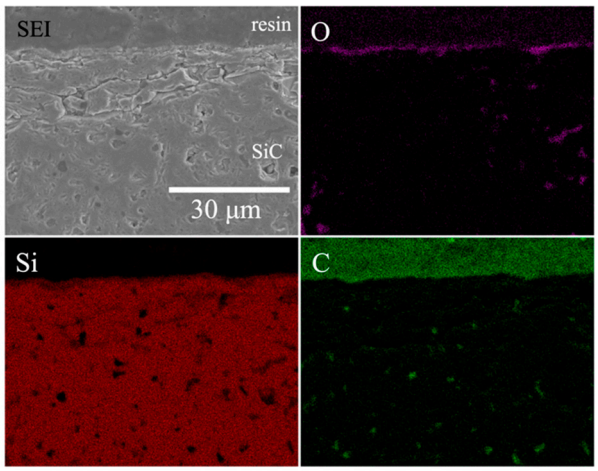

(**a**)

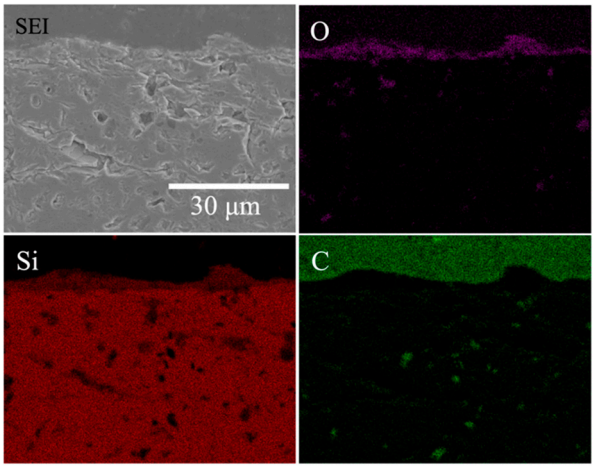

(**b**)

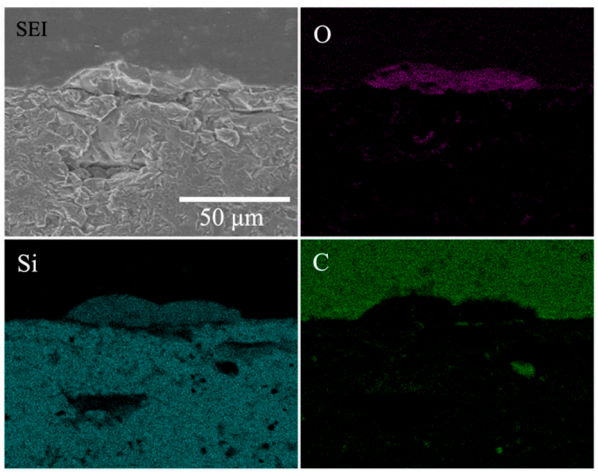

(**c**)

Figure 4. SEM–EDX results from cross-sectional view of the cylindrical samples at three different areas (**a**–**c**) after oxidation in air at 1400 °C for 10 h: SEM–EDX C, Si, and O mapping.

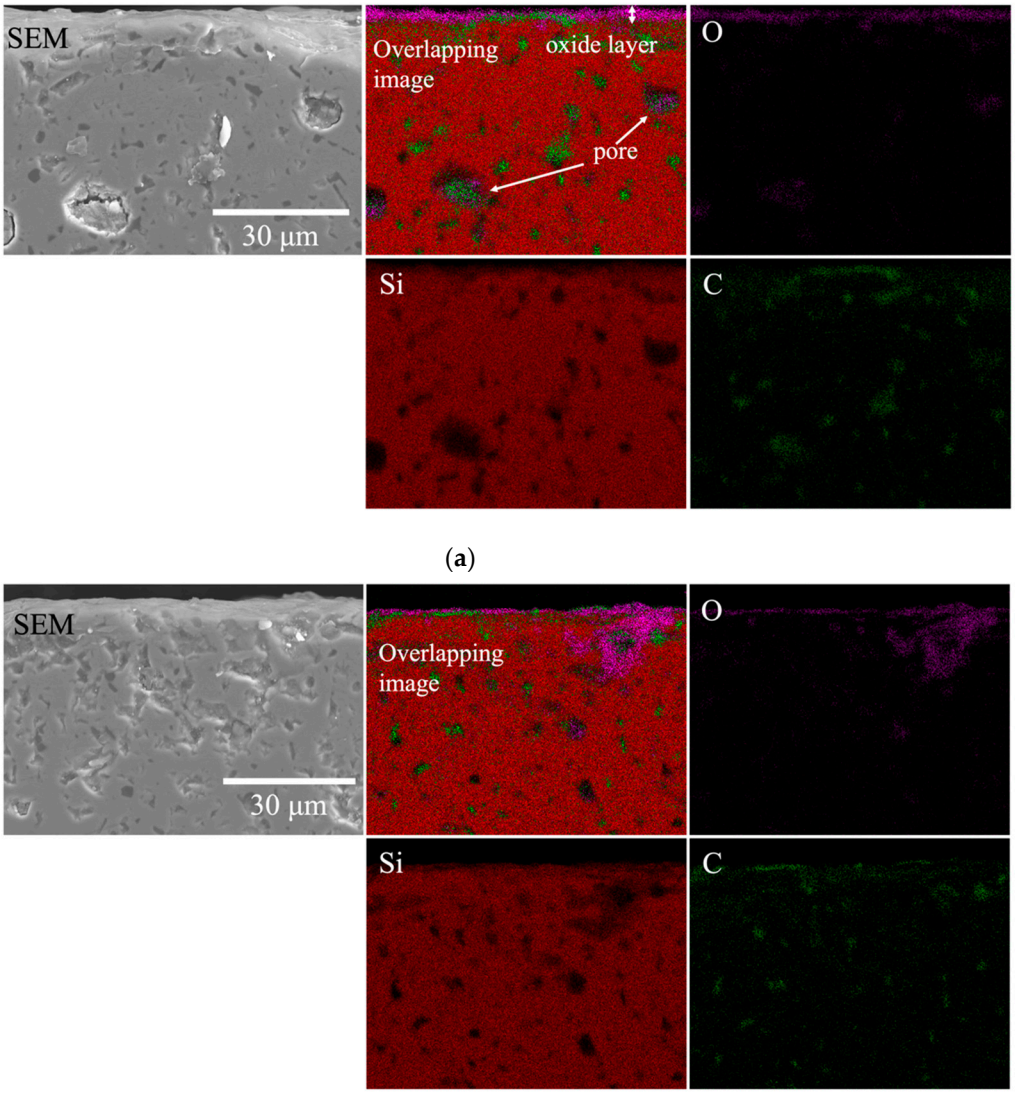

Figure 5. SEM–EDX results from cross-sectional view of the cylindrical samples at two different areas (**a**,**b**) after oxidation in air at 1200 °C for 10 h: secondary electron image (SEI) and SEM–EDX C, Si, and O mapping with overlapping image.

Next, Figure 7a,b presents mass changes in the test specimens during air oxidation at 1000–1400 °C for a 10 h duration. Each full line shows a stable mass gain process, demonstrating passive oxidation mode with parabolic-type mass gain behavior [38,39]. In the initial stage of the passive mode, the mass increases linearly (reaction-controlled regime), whereas, as time passes, the mass increases parabolically (diffusion-controlled regime). In these passive phenomena, the growth of SiO_2 contributes to the total mass gain. Obviously, the mass change rate is accelerated under elevated temperatures. The 1400 °C case has achieved the highest total mass gain at 10 h duration with minimal amount of mass loss at later stage of oxidation due to the oxidation of free carbon [8,11]. Figure 8a–c provides the mass change rates at elevated temperatures (from room temperature to each target temperature) corresponding to each measurement (Figure 7). The temperature is shown from room temperature to each targeted temperature; thus, horizontal coordinates include 10 h (at constant temperature oxidation time) and start-up time until targeted temperatures, totally exceeding 10 h. During the heating process, every case indicates a narrow peak of mass loss around 800 °C. This mass loss may be associated with the

oxidation of free carbon contained as an impurity in the specimens. Over 800 °C, the mass change rate positively increases at a higher rate (reaction-controlled regime). In a diffusion-controlled regime, the mass change rate gradually decreases and eventually approaches zero. Especially in the 1200 °C case, the mass change has completely terminated; thus, passive oxidation has stopped nevertheless during isothermal heating.

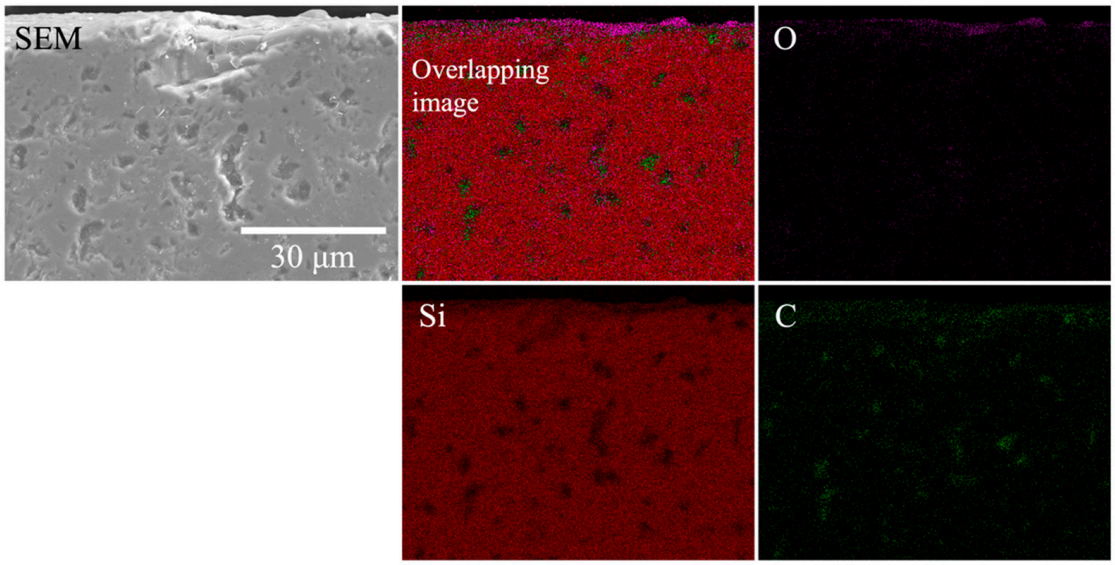

(**a**)

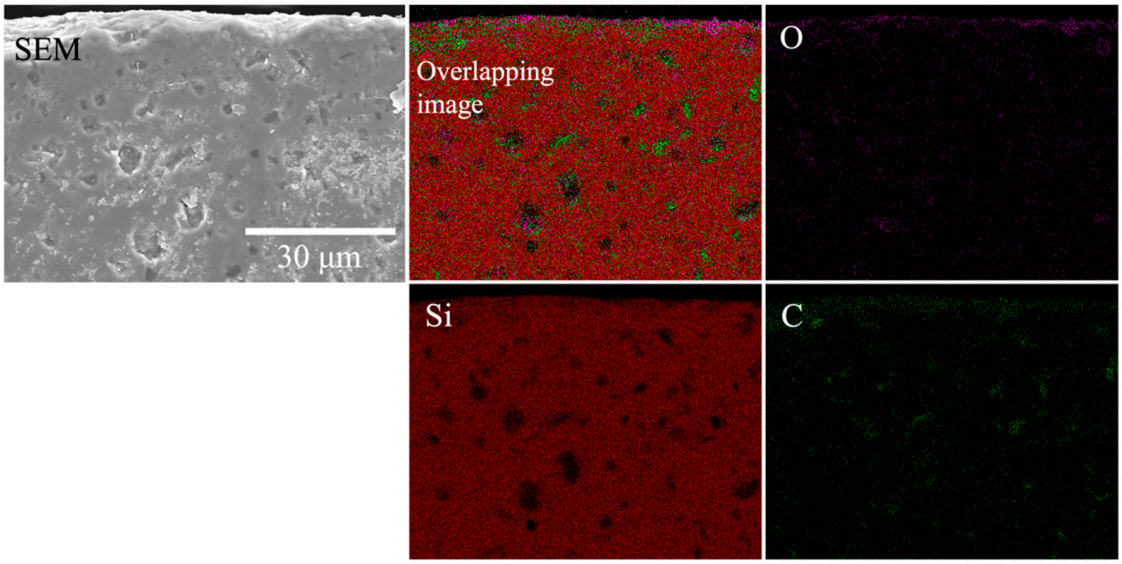

(**b**)

Figure 6. SEM–EDX results from cross-sectional view of the cylindrical samples at two different areas (**a**,**b**) after oxidation in air at 1000 °C for 10 h: secondary electron image (SEI) and SEM–EDX C, Si, and O mapping with overlapping image.

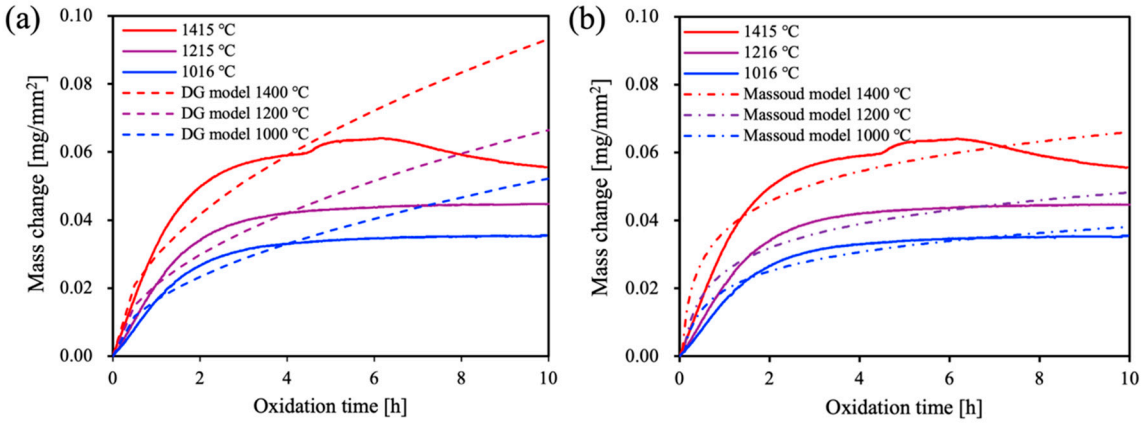

Figure 7. Empirical prediction (dotted line) compared with measured data (full line) for RS-SiC high temperature oxidation to simulate postulated air ingress accident: (**a**) Deal–Grove model, (**b**) Massoud model.

Generally, the para-linear kinetics can be described by the Deal–Grove model [40–42], which is mathematically featured as the following Equations (2) and (3):

$$\frac{dX}{dt} = \frac{B}{A + 2X} \tag{2}$$

$$\frac{B}{A} = \frac{kC_o^0}{N_0},\ B = \frac{2D_oC_o^0}{N_0} \tag{3}$$

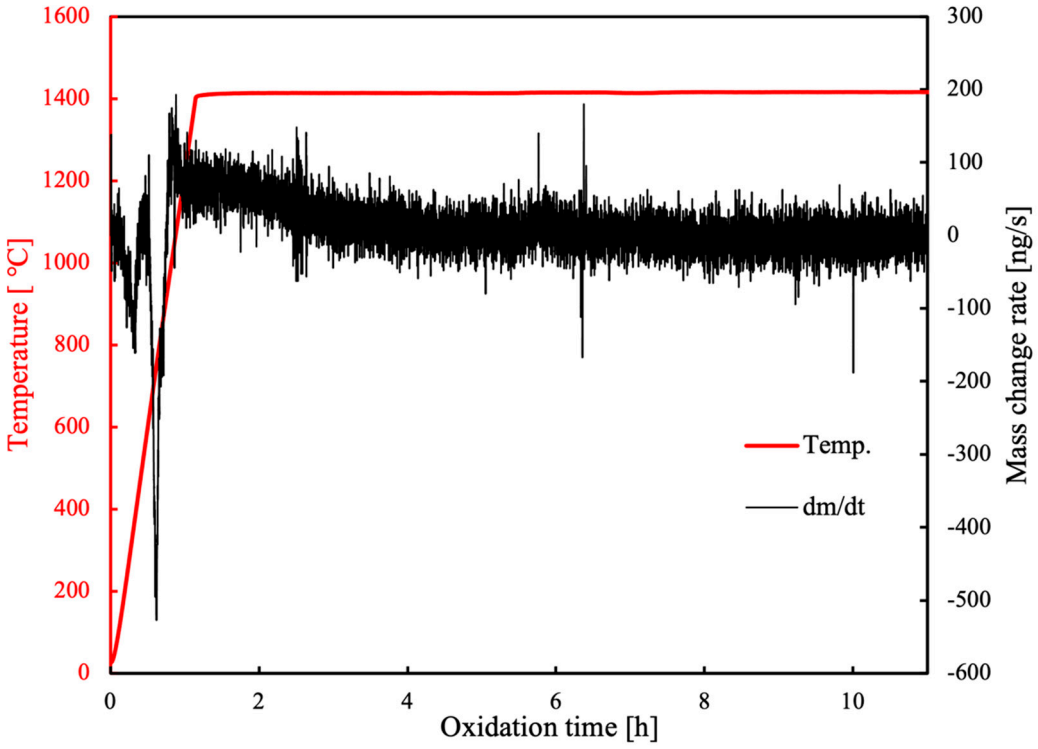

(**a**)

Figure 8. *Cont.*

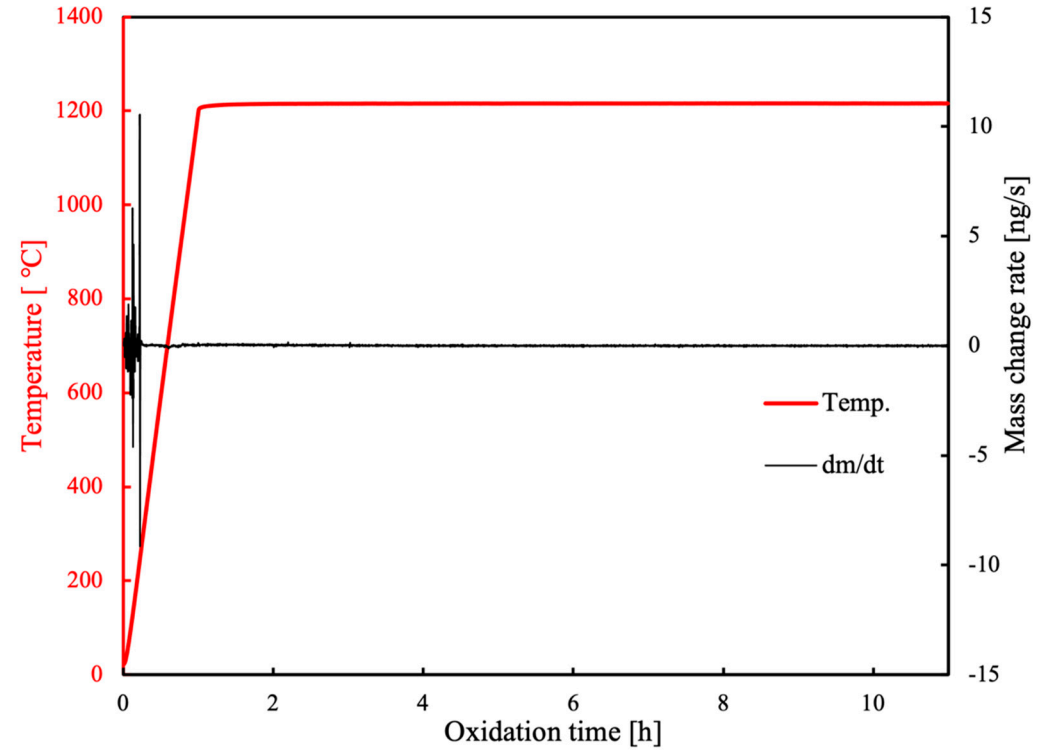

(**b**)

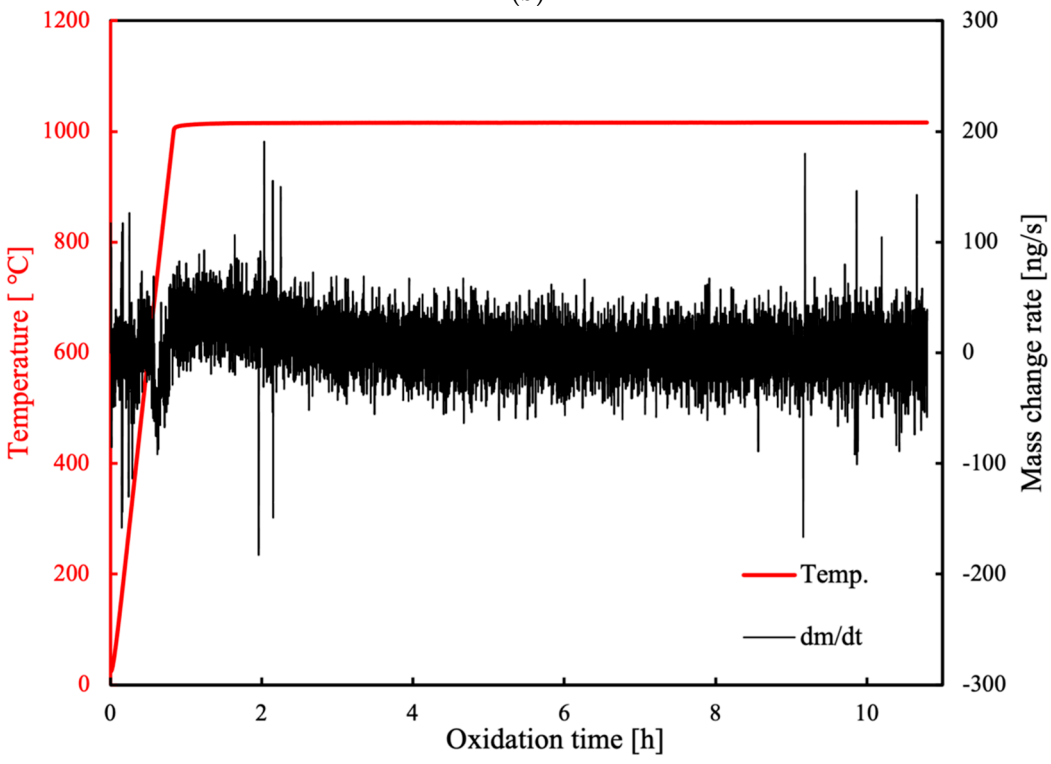

(**c**)

Figure 8. Mass change rates under elevated temperatures (from room temperature to each targeted temperature: (**a**) 1400 °C, (**b**) 1200 °C, and (**c**) 1000 °C) corresponding to each thermogravimetry measurement (Figure 7).

B/A and *B* are denoted as the linear and parabolic rate constants of oxidation, respectively. It should be noted that *B/A* and *B* are the rate coefficients for the interfacial reaction

and the diffusion of oxidants, as stated in Equation (3), where k is the interfacial oxidation rate constant, C_o *is* the limit of solubility in SiO_2, N_0 *is* the molecular density of SiO_2, D is the diffusivity in SiO_2, and the subscript means the value of the corresponding atom. This model argues that the oxidation is suppressed by the diffusion-controlled mechanism of oxygen; thus, the oxidation rate is reduced as the time passes. Based on this theory, the mass gain continuously occurs as a parabolic behavior even at lower rates. In the present results, however, oxidation behavior may not have reproduced the typical para-linear kinetics. When applying the DG model to the obtained result, the total mass gain indicates large differences between the prediction of the DG model and the measured data at 10 h (Figure 7a). In fact, the DG model and its related models [43–45] were originally developed to simulate the initial stage of oxidation. Focusing on the very initial stage of mass changes, the DG model has predicted the measured data well. Although the oxidation nearly ended at 4 h duration, the DG model predicts a higher mass gain rate in parabolic law. Since the current DG model is likely to overestimate the RS-SiC mass changes during long-term observation, it is not suitable for estimating oxidation in the RS-SiC fuel matrix over durations of several hundred hours [46] during the air ingress event. Here are other potential models that support the present result. Massoud et al. have reported that the oxidation rate depends on the oxide thickness [47,48]. They have successfully modified the DG model by adding an exponential term as follows (Equation (4)):

$$\frac{dX}{dt} = \frac{B}{A + 2X} + C \exp\left(-\frac{X}{L}\right) \quad (4)$$

where C and L are the pre-exponential constant and the characteristic length, respectively. In this empirical relation, they have tried to decelerate the oxidation rate depending on the oxide growth. Another previous example has proposed an interfacial Si and C emission model [49] to reduce the oxidation rate at the SiO_2/SiC interface due to the accumulation of out-warding Si and C atoms. In this theory, Hijikata et al. have argued that the oxide growth rate can be a function of oxide thickness. Some plots indicate that the oxide growth rate decreases as the oxide thickness increases [49] and may saturate at 20 nm for oxidation of the C face.

As introduced so far, several studies have measured the oxidation rate for different types of SiC; this work has found that the DG model may need a minor correction to adequately estimate the oxide growth during a longer period as well. According to this hypothesis, Massoud's model has been applied to our measurements (Figure 7b). The modification has produced higher errors at the initial stage of oxidation compared to the DG model; however, the Massoud model has shown better agreement with the measured data in the total mass gain within the error range of 18.9, 7.71, and 7.37% at 1400, 1200, and 1000 °C, respectively. Throughout the present analysis, it may be suggested that the passive oxidation rate (or oxide growth rate) decelerates depending on the oxide thickness at the targeted temperatures and may converge to zero when the terminal thickness is reached.

4. Conclusions

This study investigated the oxide-growth mechanisms of the SiC fuel matrix under postulated air ingress accident conditions for fuel safety evaluation. TGA was used to monitor the oxidation kinetics, resulting in an oxide growth model that accurately fits the measured data. The SEM–EDX observations identified the oxide structures at various temperatures, enabling the estimation of oxide thickness and the prediction of corrosion resistance. These findings confirm that the SiC fuel matrix maintains its durability against corrosion up to 1400 °C for 10 h without any unacceptable morphological changes. The oxide growth mechanisms of the RS-SiC during the accident are elucidated, referring to several theoretical models.

Author Contributions: Conceptualization, Y.N.; methodology, Y.N. and A.G.; investigation, Y.N. and A.G.; data curation, Y.N. and A.G.; writ-ing-original draft preparation, Y.N.; writing-review and

editing, A.G.; super-vision, K.Y.; project administration, K.O.; funding acquisition, K.O. All authors have read and agreed to the published version of the manuscript.

Funding: This study was supported in part by the MEXT Innovative Nuclear Research and Development Program (Grant Number JPMXD21457197).

Data Availability Statement: Dataset available on request from the authors.

Conflicts of Interest: The authors declare no conflict of interest.

References

1. Kruminš, J.; Klavinš, M. Investigating the Potential of Nuclear Energy in Achieving a Carbon-Free Energy Future. *Energies* **2023**, *16*, 3612. [CrossRef]
2. IAEA. Safety related design and economic aspects of HTGRs. In Proceedings of the Technical Committee Meeting, Beijing, China, 24 November 1998; IAEA-TECDOC-1210.
3. Fukaya, Y.; Goto, M.; Ohashi, H.; Tachibana, Y.; Kunitomi, K.; Chiba, S. Proposal of a plutonium burner system based on HTGR with high proliferation resistance. *J. Nucl. Sci. Technol.* **2014**, *51*, 818–831. [CrossRef]
4. Ohashi, H.; Sato, H.; Yan, X.L.; Sumita, J.; Nomoto, Y.; Tazawa, Y.; Noguchi, H.; Imai, Y.; Tachibana, Y. *Conceptual Design of Small-Sized HTGR System-Plant Design and Technical Feasibility*; JAEA-Technology 2013-016; Japan Atomic Energy Agency: Ibaraki, Japan, 2013.
5. Huning, A.J.; Chandrasekaran, S.; Garimella, S. A review on recent advances in HTGR CFD and thermal fluid analysis. *Nucl. Eng. Design* **2021**, *373*, 111013. [CrossRef]
6. Yamashita, K.; Shindo, R. Nuclear design of the high-temperature engineering test reactor (HTTR). *Nucl. Sci. Eng.* **1996**, *122*, 212–228. [CrossRef]
7. Inaba, Y.; Nishihara, T. Development of fuel temperature calculation code for HTGRs. *Ann. Nucl. Energy* **2017**, *101*, 383–389. [CrossRef]
8. Nishimura, Y.; Gubarevich, A.; Yoshida, K.; Okamoto, K. Comparison of SiC and graphite oxidation behavior under conditions of HTGR air ingress accident. *Mech. Eng. Lett.* **2022**, *8*, 22–00315.
9. Okita, S.; Mizuta, N.; Takamatsu, K.; Goto, M.; Yoshida, K.; Nishimura, Y.; Okamoto, K. Research on improvement of HTGR core power-density: (4) feasibility study for a reactor core. In Proceedings of the 30th International Conference on Nuclear Engineering, Kyoto, Japan, 21–26 May 2023.
10. Nishimura, Y.; Gubarevich, A.; Yoshida, K.; Sharma, A.K.; Okamoto, K. Kinetic modelling of IG-110 oxidation in inert atmosphere with low oxygen concentration for innovative high-temperature gas-cooled reactor applications. *Nucl. Sci. Technol* **2023**, *61*, 802–809. [CrossRef]
11. Sharma, A.K.; Sagawa, W.; Ahmed, Z.; Nishimura, Y.; Okamoto, K. Integrated experimental assessment and validation of oxidation with real-scale SiC fuel compact in HTGR. *Int. J. Heat Mass Transf.* **2024**, *220*, 124930. [CrossRef]
12. Nishimura, Y.; Gubarevich, A.; Yoshida, K.; Sharma, A.K.; Okamoto, K. Modeling passive/active transition in high-temperature dry oxidation of reaction-sintered SiC for innovative fuel matrix in high-temperature gas-cooled reactors. *J. Eur. Ceram. Soc.* **2024**, *44*, 3031–3038. [CrossRef]
13. Snead, L.L.; Nozawa, T.; Katoh, Y.; Byun, T.S.; Kondo, S.; Petti, D.A. Handbook of SiC properties for fuel performance modeling. *J. Nucl. Mater.* **2007**, *371*, 329–377. [CrossRef]
14. Hishida, M.; Takeda, T. Study on air ingress during an early stage of a primary-pipe rupture accident of a high-temperature gas-cooled reactor. *Nucl. Eng. Des.* **1991**, *126*, 175–187. [CrossRef]
15. Takeda, T. Air ingress phenomena in a depressurization accident of the very-high-temperature reactor. *High Temp. React. Technol.* **2008**, *48548*, 633–640.
16. Oh, C.H.; Kang, H.; Kim, E.S. Air-ingress analysis: Part 2—Computational fluid dynamic models. *Nucl. Eng. Des.* **2011**, *241*, 213–225. [CrossRef]

17. Yanhua, Z.; Fubing, C.; Lei, S. Analysis of diffusion process and influence factors in the air ingress accident of the HTR-PM. *Nucl. Eng. Des.* **2014**, *271*, 397–403. [CrossRef]
18. Xu, W.; Shi, L.; Zheng, Y. Transient analysis of nuclear graphite oxidation for high temperature gas cooled reactor. *Nucl. Eng. Des.* **2016**, *306*, 138–144. [CrossRef]
19. Liu, P.; Chen, Z.; Zheng, Y.; Sun, J.; Chen, F.; Shi, L.; Zhang, Z. Study on air ingress of the 200 MWe pebble-bed modular high temperature gas-cooled reactor. *Ann. Nucl. Energy* **2016**, *98*, 120–131. [CrossRef]
20. Raine, M. Effect of Delays in Afterheat Removal on Consequences of Massive Air Ingress Accidents in High-Temperature Gas Cooled Reactors. *J. Nucl. Sci. Technol.* **1984**, *21*, 824–835.
21. Elfrida, S.; Roziq, H. Study of oxidation effects on HTGR graphite in air ingress accidents condition. *AIP Conf. Proc.* **2019**, *2180*, 020013.
22. Braun, J.; Gueneau, C.; Alpettaz, T.; Sauder, C.; Brackx, E.; Domenger, R.; Gossé, S.; Balbaud-Célérier, F. Chemical compatibility between UO_2 fuel and SiC cladding for LWRs. Application to ATF (Accident-Tolerant Fuels). *J. Nucl. Mater.* **2017**, *487*, 380–395. [CrossRef]
23. Kim, D.; Lee, H.G.; Park, J.Y.; Park, Y.Y.; Kim, W.J. Effect of dissolved hydrogen on the corrosion behavior of chemically vapor deposited SiC in a simulated pressurized water reactor environment. *Corros. Sci.* **2015**, *98*, 304–309. [CrossRef]
24. Snead, L.L.; Venneri, F.; Kim, Y.; Terrani, K.A.; Tulenko, J.E.; Forsberg, C.W. Fully ceramic microencapsulated fuels: A transformational technology for present and next generation reactors. *ANS Trans.* **2011**, *104*, 6.
25. Powers, J.J.; Lee, W.J.; Venneri, F.; Snead, L.L.; Jo, C.K.; Hwang, D.H.; Terrani, K.A. *Fully Ceramic Microencapsulated (FCM) Replacement Fuel for LWRs*; National Technical Information Service: Springfield, VA, USA, 2013; ORNL/TM-2013/173.
26. Dai, X.; Cao, X.; Yu, S.; Zhu, C. Conceptual core design of an innovative small PWR utilizing fully ceramic microencapsulated fuel. *Prog. Nucl. Energy* **2009**, *75*, 63–71. [CrossRef]
27. Kamalpour, S.; Salehi, A.A.; Khalafi, H.; Mataji-Kojouri, N.; Jahanfarnia, G. The potential impact of Fully Ceramic Microencapsulated (FCM) fuel on thermal hydraulic performance of SMART reactor. *Nucl. Eng. Des.* **2018**, *339*, 39–52. [CrossRef]
28. Terrani, K.A.; Kiggans, J.O.; Katoh, Y.; Shimoda, K.; Montgomery, F.C.; Armstrong, B.L.; Snead, L.L. Fabrication and characterization of fully ceramic microencapsulated fuels. *J. Nucl. Mater.* **2012**, *426*, 268–276. [CrossRef]
29. Kiegiel, K.; Herdzik-Koniecko, I.; Fuks, L.; Zakrzewska-Kołtuniewicz, G. Management of Radioactive Waste from HTGR Reactors including Spent TRISO Fuel—State of the Art. *Energies* **2022**, *15*, 1099. [CrossRef]
30. Guittonneau, F.; Abdelouas, A.; Grambow, B. HTR Fuel Waste Management: TRISO Separation and Acid-Graphite Intercalation Compounds Preparation. *J. Nucl. Mater.* **2010**, *407*, 71–77. [CrossRef]
31. Roy, J.; Chandra, S.; Das, S.; Maitra, S. Oxidation behaviour of silicon carbide-a review. *Rev. Adv. Mater. Sci* **2014**, *38*, 29–39.
32. Chatillon, C.; Teyssandier, F. Thermodynamic assessment of the different steps observed during SiC oxidation. *J. Eur. Ceram. Soc.* **2022**, *42*, 1175–1196. [CrossRef]
33. Tanaka, H. Silicon carbide powder and sintered materials. *J. Ceram. Soc. Jpn.* **2011**, *119*, 218–233. [CrossRef]
34. Omori, M.; Takei, H. Pressureless sintering of SiC. *J. Amer. Ceram. Soc.* **1982**, *65*, 92–96. [CrossRef]
35. Osborne, M.; Hay, J.C.; Snead, L.L. Mechanical- and physical-property changes of neutron-irradiated chemical-vapor-deposited silicon carbide. *J. Amer. Ceram. Soc.* **1999**, *82*, 2490–2496. [CrossRef]
36. Popper, P. (Ed.) The preparation of dense self bonded silicon carbide. In *Special Ceramics*; Heywood: London, UK, 1960; pp. 209–219.
37. Terrani, K.A.; Snead, L.L.; Gehin, J.C. Microencapsulated fuel technology for commercial light water and advanced reactor application. *J. Nucl. Mater.* **2012**, *427*, 209–224. [CrossRef]
38. Gould, D.; Franken, D.; Bindra, H.; Kawaji, M. Transition from molecular diffusion to natural circulation mode air-ingress in high temperature helium loop. *Ann. Nucl. Energy* **2017**, *107*, 103–109. [CrossRef]
39. Das, D.; Farjas, J.; Roura, P. Passive-Oxidation Kinetics of SiC Microparticles. *J. Am. Ceram. Soc.* **2004**, *87*, 1301–1305. [CrossRef]
40. Deal, B.E.; Grove, A.S. General Relationship for the Thermal Oxidation of Silicon. *J. Appl. Phys.* **1965**, *36*, 3770–3778. [CrossRef]
41. Kim, D.H.; Kim, K.K.; Moon, B.W.; Park, K.B.; Park, S.; Seok, C.S. Prediction of growth behavior of thermally grown oxide considering the microstructure characteristics of the top coating. *Ceram. Int.* **2021**, *47*, 14160–14167. [CrossRef]
42. Ramachandran, K.; Chaffey, B.; Zuccarini, C.; Bear, J.C.; Jayaseelan, D.D. Experimental and mathematical modelling of corrosion behavior of CMAS coated oxide/oxide CMCs. *Ceram. Int.* **2023**, *49*, 4213–4221. [CrossRef]
43. Kageshima, H.; Shiraishi, K.; Uematsu, M. Universal Theory of Si Oxidation Rate and Importance of Interfacial Si Emission. *Jpn. J. Appl. Phys.* **1999**, *38*, 971–974. [CrossRef]
44. Ogawa, S.; Takakuwa, Y. Rate-Limiting Reactions of Growth and Decomposition Kinetics of Very Thin Oxides on Si (001) Surfaces Studied by Reflection High-Energy Electron Diffraction Combined with Auger Electron Spectroscopy. *Jpn. J. Appl. Phys.* **2006**, *45*, 7063–7079. [CrossRef]
45. Uematsu, M.; Kageshima, H.; Shiraishi, K. Simulation of wet oxidation of silicon based on the interfacial silicon emission model and comparison with dry oxidation. *J. Appl. Phys.* **2001**, *89*, 1948–1953. [CrossRef]
46. Du, B.; Li, H.; Zheng, W.; He, X.; Ma, T.; Yin, H. Study of oxidation behavior and tensile properties of candidate superalloys in the air ingress simulation scenario. *Nucl. Eng. Technol.* **2023**, *55*, 71–79. [CrossRef]
47. Massoud, H.Z.; Plummer, J.D.; Irene, E.A. Thermal Oxidation of Silicon in Dry Oxygen: Growth-Rate Enhancement in the Thin Regime: I. Experimental Results. *J. Electrochem, Soc.* **1985**, *132*, 2685–2693. [CrossRef]

48. Massoud, H.Z.; Plummer, J.D.; Irene, E.A. Thermal Oxidation of Silicon in Dry Oxygen: Growth-Rate Enhancement in the Thin Regime: II. Physical Mechanism. *J. Electrochem, Soc.* **1985**, *132*, 2693–2700. [CrossRef]
49. Hijikata, Y.; Yamaguchi, H.; Yoshida, S. A Kinetic Model of Silicon Carbide Oxidation Based on the Interfacial Silicon and Carbon Emission Phenomenon. *Appl. Phys. Express* **2009**, *2*, 021203-1–021203-3. [CrossRef]